Available online at www.sciencedirect.com
ScienceDirect
Journal of Nuclear Materials 361 (2007) 248–261
journal of nuclear materials
www.elsevier.com/locate/jnucmat

APT characterization of irradiated high nickel RPV steels

M.K. Miller [a,*], K.F. Russell [a], M.A. Sokolov [b], R.K. Nanstad [b]

[a] Microscopy Group, Materials Science and Technology Division, Oak Ridge National Laboratory, P.O. Box 2008, Building 4500S, MS 6136, Oak Ridge, TN 37831-6136, United States

[b] Nuclear Materials Science and Technology Group, Materials Science and Technology Division, Oak Ridge National Laboratory, P.O. Box 2008, Building 4500S, MS 6136, Oak Ridge, TN 37831-6136, United States

Abstract

Samples of the welds from the Midland and Palisades reactors in the unirradiated condition and after neutron irradiation to a high fluence of up to 3.4×10^{23} m^{-2} ($E > 1$ MeV) have been characterized with the Oak Ridge National Laboratory's local electrode atom probe. High number densities, ~5 and $\sim 7 \times 10^{23}$ m^{-3}, respectively, of ~2-nm-diameter copper-, nickel-, manganese- and silicon-enriched precipitates were observed after neutron irradiation. These copper-enriched precipitates were observed both in the matrix of the steel and also preferentially located along the dislocations. No appreciable differences were observed in the sizes or the compositions of the precipitates in the matrix and on the dislocations. The average interparticle distance along the dislocations was 11 ± 3 nm. Phosphorus segregation was also evident along the dislocations in both welds. No other nanoscale intragranular phases were observed in these neutron irradiated welds.

PACS: 61.82.Bg; 62.20.Mk; 81.40.−z

1. Introduction

The purposes of this study were to investigate the influence of high nickel levels on the response to neutron irradiation of high copper pressure vessel steel welds and to establish whether any additional phases were present after neutron irradiation. The materials used in this study were a high nickel and high copper content pressure vessel steel weld from the Palisades reactor and a high copper content weld from the Midland reactor. The nickel level in the Palisades weld was at least twice the average of that typically found in Western pressure vessel steels. Nickel is added to reactor pressure vessel (RPV) steels to increase hardenability and decrease the ductile–brittle transition temperature. It is generally accepted that the presence of nickel in these RPV steels also increases their sensitivity to neutron induced embrittlement even at low phosphorus and copper concentrations [1–3]. However, the mechanisms controlling the damage process are not well understood. Microstructural studies of several neutron irradiated RPV steels have shown clear evidence of nickel in the irradiation-induced copper-enriched precipitates, a copper–nickel synergistic effect and, more recently, a nickel–manganese

* Corresponding author. Tel.: +1 865 574 4719; fax: +1 865 241 3650.
E-mail address: millermk@ornl.gov (M.K. Miller).

0022-3115/$ - see front matter © 2006 Elsevier B.V. All rights reserved.
doi:10.1016/j.jnucmat.2006.12.015

synergistic effect [4–8]. Because of the significance of transition temperature shift predictions for RPV integrity assessments, it is of great importance to investigate the mechanisms of neutron embrittlement of light-water RPV steels containing high nickel contents, especially weld metals, including those typical of Mn–Ni–Cr–Mo pressurized water reactors.

The microstructures of these welds from the two pressure vessel steels have been characterized after neutron irradiation to a fluence of up to 3.4×10^{23} n m^{-2} ($E > 1$ MeV) by atom probe tomography [9,10]. The highest fluence investigated was a high level of irradiation for a pressurized water reactor (PWR) pressure vessel and is a level near the end-of-life of the reactor. Atom probe tomography has been used previously to characterize several neutron irradiated RPV steels and model alloys including some characterizations of the weld material from the Palisades and Midland reactors [11–25]. The change in the copper solubility in the matrix of a submerged arc beltline weld (designated a Babcock and Wilcock WF-70 weld) from the Midland reactor after exposure to a fluence of 1.1×10^{23} n m^{-2} ($E >$ 1 MeV), and also thermal annealing experiments have been reported previously [24]. Atom probe analysis revealed a substantial depletion in the copper content of the matrix after the stress relief treatment to 0.119 ± 0.007 at.% Cu with a further depletion to 0.058 ± 0.008 at.% Cu together with the precipitation of some ultrafine copper-enriched precipitates after neutron irradiation. Thermal annealing of the irradiated weld for 168 h at 454 °C further reduced the copper content to 0.05 ± 0.01 at.% Cu. This study concluded that the post irradiation anneal further depletes the copper content of the matrix rather than dissolving the precipitates and increasing the copper content in the matrix thereby reducing but not necessarily eliminating the susceptibility of the material to further embrittlement from the copper-enriched precipitates during subsequent irradiation.

A local electrode atom probe characterization of the Palisades weld that was irradiated in the Ford reactor at a temperature of 288 °C and a flux of $\sim 7 \times 10^{15}$ m^{-2} s^{-1} to a fluence of 1.4×10^{23} n m^{-2} ($E > 1$ MeV) has also been reported [25]. Atom probe tomography of the neutron irradiated Palisades weld revealed a high number density of ~2-nm-diameter copper-, nickel-, manganese-, silicon- and phosphorus-enriched precipitates and phosphorus segregation to dislocations [25].

2. Materials and specimens

Two different types of pressure vessel steel welds with low and high nickel contents and high copper contents were selected for this study.

The first type of pressure vessel steel was a high copper (0.20 wt% Cu) high nickel (1.20 wt%) weld from the Palisades reactor. The average composition of the Palisades weld is listed in Table 1. The nickel level in the Palisades weld is the maximum nickel level given in Reg. Guide 1.99 Rev. 2. This steam generator weld with the same weld description as that of the reactor pressure vessel was fabricated with a submerged-arc welding process with weld wire (heat 34B009) with a nickel addition (Ni-200 heat number N7753A), and a Linde 1092 welding flux (Lot No. 3708). It was post weld heat treated in the range 593–627 °C for ~14 h. The Palisades weld was irradiated in the Ford reactor at a temperature of 288°C and a flux of $\sim 7 \times 10^{15}$ m^{-2} s^{-1} to a fast fluence of 3.4×10^{23} n m^{-2} ($E > 1$ MeV). This condition is an accelerated irradiation by more than an order of magnitude.

The second pressure vessel steel was a high copper, medium nickel beltline weld from the Midland reactor. The compositional variation of this weld as a function of distance through the weld [0.21–0.32 wt% Cu (0.18–0.28 at.% Cu)] has been reported previously [24]. The nickel content of this weld was 0.58–0.63 wt% Ni (0.55–0.59 at.% Ni). The average composition of the Midland weld is listed in Table 1. In addition to the lower nickel level of this weld, it is also higher in manganese, silicon and chromium and lower in molybdenum. Prior to irradiation, the

Table 1
Nominal compositions of the welds from the Midland and Palisades reactors

Element	Midland reactor weld		Palisades reactor weld	
	wt%	at.%	wt%	at.%
	#2–#5	#2–#5		
Cu	0.21–0.32	0.18–0.28	0.20	0.18
Ni	0.61–0.60	0.58–0.57	1.20[a]	1.14
Mn	1.45–1.61	1.46–1.62	1.27	1.29
Si	0.65–0.67	1.28–1.32	0.18	0.36
Cr	0.14–0.11	0.15–0.12	0.04	0.04
Mo	0.42–0.41	0.4–0.24	0.55	0.32
C	0.11–0.08	0.51–0.36	0.11	0.51
P	0.018–0.022	0.032–0.039	0.014	0.03

The values for the Midland reactor are from the low and high copper positions 2 and 5. The balance is iron.
[a] Nickel level limit of Reg. Guide 1.99 Rev. 2.

pressure vessel was subjected to a standard post weld heat treatment of 22.5 h at 607 ± 14 °C. This weld was also neutron irradiated to a fluence of 3.4×10^{23} n m^{-2} ($E > 1$ MeV) at a temperature of 288 °C.

These alloys were characterized with the Oak Ridge National Laboratory's local electrode atom probe. Samples for local electrode atom probe characterization were cut from the weld section of Charpy bars and electropolished into needle shaped specimens with the use of standard methods [9,10]. A specimen temperature of 50 K, a pulse repetition rate of 200 kHz and a pulse fraction of 20% were used for the atom probe analyses. All compositions quoted in this report are given in atomic percent.

The local electrode atom probe permits the elemental identities and the position coordinates of the atoms in a small volume of a specimen containing up to ~100 million atoms to be determined with atomic precision. Therefore, the local configuration of atoms in this volume with near atomic spatial resolution may be investigated for the earliest stages of phase separation [9]. Although the term precipitate is used here to describe the ultrafine copper-enriched regions, several other terms such as clusters, nanoclusters or atmospheres could also be used. It should not be inferred from this terminology that these features are thermodynamically stable or at equilibrium.

The existence of features produced by irradiation-assisted phase separation such as embryos or ultrafine precipitates may be located in the three-dimensional data by searching for those atoms that are within a certain distance of another solute atom of the same type or group of types [9]. This maximum separation or friends-of-friends (FOF) method enables the solutes in the ultrafine precipitates to be distinguished from the solutes in the matrix so that their size, composition and number density can be estimated [9,14]. The magnitude of the typical separation distance, d_{max}, depends on the solute concentrations in the precipitates and the matrix and is generally of the order of a few nearest neighbor distances (i.e., ~0.3 to ~0.7 nm) [26,27]. Since the solute atoms in the matrix of a dilute solid solution such as the copper atoms in a pressure vessel steel are generally further apart than this distance, the solute in the matrix is eliminated. This method detects solute agglomerations containing two or more atoms of interest. However, some of the smaller agglomerations are due to the solute distribution in a random solid solution. Therefore, a minimum size cutoff limit, n_{min}, is estimated either from the analyses of APT data from a solid solution or from a simulation of random solid solution with the same parameters as the alloy under investigation including the matrix solute level, atomic density (i.e., crystal structure and lattice parameters) and detection efficiency of the mass spectrometer (~50%) [26,27]. This estimate of the cutoff limit is an upper limit since when phase separation occurs the solute level in the matrix decreases resulting in an increase in the separation of similar atoms in the matrix. Consequently, the size distribution and number density of the precipitates present due to the random distribution of solute will also decrease.

Some of these embryos will be transient and the solute associated with them will return to the solid solution and form other embryos with time. However, their presence is important in understanding the mechanical properties of the alloy, because they will impede the motion of dislocations and can be considered as an additional component to the matrix hardening. Therefore, they should be taken into account in models that estimate the amount of embrittlement that occurs in these materials.

The center of mass, the radius of gyration, l_g, and the Guinier radius, r_G, may be estimated directly from the coordinates of the solute atoms in each precipitate [9]. The number density, N_v, may be estimated from the number of precipitates in the analyzed volume after taking into account clipping with the volume extents [9]. Comparison of these parameters with those derived from small angle neutron scattering experiments on the same materials has shown excellent agreement in other pressure vessel steels [27].

Several methods may be used to determine the composition of ultrafine features from atom probe data. In the envelope method used in this study, a three-dimensional grid of volume elements containing the number of atoms of all elements may be constructed from the volume elements corresponding to the positions of the selected atom species [9]. To retain the inherent spatial resolution of the APT technique, the grid spacing is less than 0.2 nm. The solute concentrations may be determined by counting the number of atoms of each element within this three-dimensional envelope. If the features are spherical, radial concentration profiles from the center of mass into the surrounding matrix may also be constructed to investigate interfacial segregation of the different solutes as shown below.

At the size range of the precipitates found in these materials, i.e., less than 5 nm diameter, the composition estimates are strongly dependent on the definition of the position of the interface between the precipitate and the matrix, the solute gradient into the matrix, the roughness of this interface on an atomic scale, and the presence and extent of interfacial segregation of all solutes. Therefore, the estimates used in this study are estimates of the solute concentrations at the core of the precipitates and should not be used for mass balance calculations.

3. Results

3.1. Fracture toughness

The Charpy impact ΔT_{41J} shifts of the Midland baseline weld after neutron irradiation to fluences of 0.5, 1.0 and 3.4×10^{23} n m^{-2} ($E>1$ MeV), Fig. 1, were 45, 103 and 108 °C, respectively. The upper shelf energy for the unirradiated weld was 88.5 J and 77 J after neutron irradiation to a fluence of 3.4×10^{23} n m^{-2} ($E>1$ MeV). Surprisingly, no significant additional increase in the ductile-to-brittle transition temperature and no additional drop in upper-shelf energy was observed after increasing the fluence from 1.0 to 3.4×10^{23} n m^{-2} ($E>1$ MeV). The fracture toughness T_0 shifts were 78, 81 and 117 °C, respectively, for neutron fluences of 0.5, 1.0 and 3.4×10^{23} m^{-2} ($E>1$ MeV).

The results of fracture toughness tests for the Palisades weld that was neutron irradiated to a fluence of 1.4×10^{23} n m^{-2} ($E>1$ MeV) revealed that the shift in the ductile-to-brittle transformation temperature from Charpy impact tests was $\Delta T_{41J}=102$ °C, as shown in Fig. 2. This value is significantly lower than the prediction from Regulatory Guideline 1.99 revision 2 (RG1.99-2) of 154 °C. The decrease in the upper shelf energy was $\Delta\text{USE}=-26$ J. After neutron irradiation to a higher fluence of 3.4×10^{23} n m^{-2} ($E>1$ MeV), $\Delta T_{41J}=149$ °C and $\Delta\text{USE}=48.5$ J. This represents an additional ΔT_{41J} shift of 47 °C and an additional drop in USE of 22.5 J. This value of $\Delta T_{41J}=149$ °C is also significantly lower than the prediction of 180 °C from RG1.99-2. However, the experimentally observed ΔT_{41J} shift was significantly higher, i.e., 31 °C, than that observed in the weld from the Midland reactor that was irradiated to the same fluence of 3.4×10^{23} n m^{-2} ($E>1$ MeV). The fracture toughness T_0 value for the unirradiated weld from the Palisades reactor was −90 °C, and 15 °C and 54 °C after neutron irradiation to fluences of 1.4 and 3.4×10^{23} n m^{-2} ($E>1$ MeV), respectively. Therefore, the shifts in T_0 were 105 and 144 °C, respectively for the two irradiated materials. The experimentally observed T_0 shift for the weld for

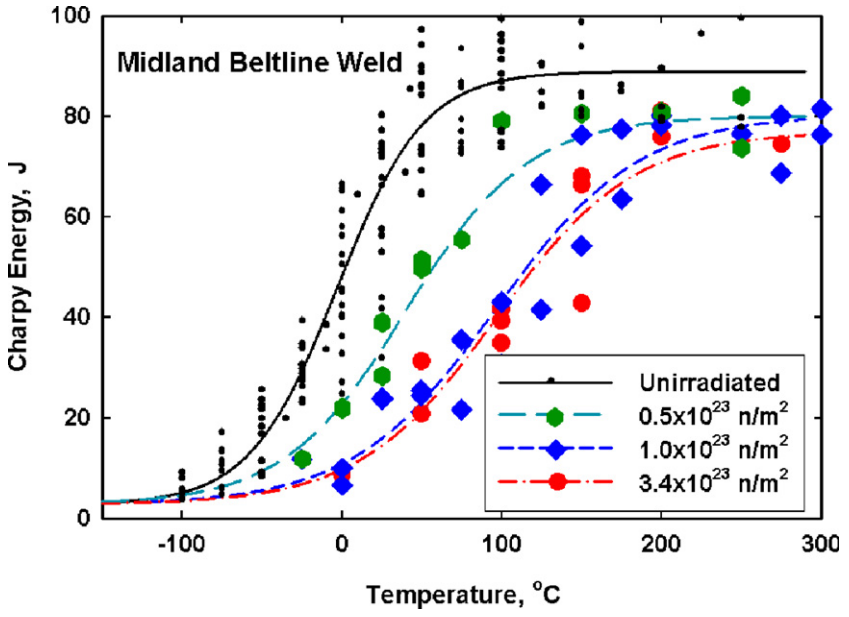

Fig. 1. The Charpy impact energies of the beltline weld from the Midland reactor as a function of temperature for the unirradiated and irradiated conditions at neutron fluences of 0.5, 1.0 and 3.4×10^{23} n m^{-2}.

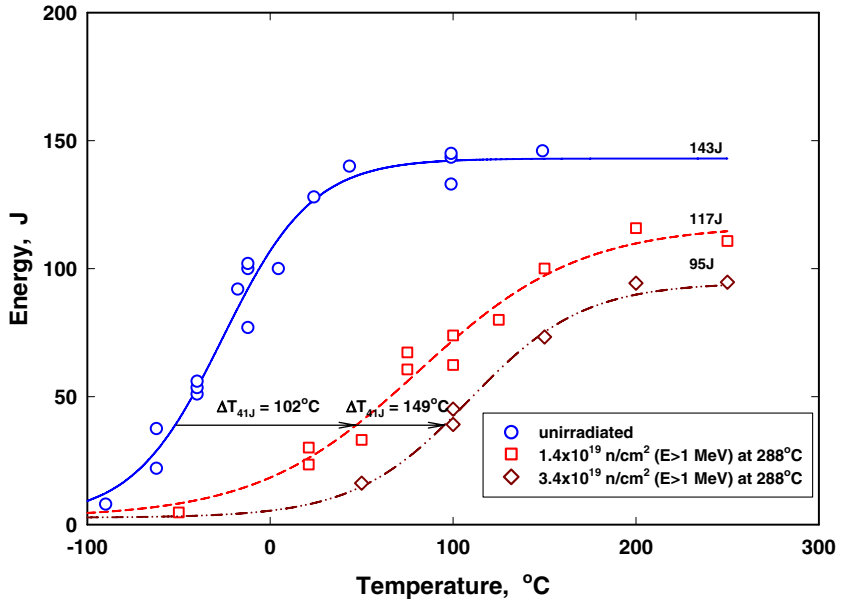

Fig. 2. The Charpy impact energies of the weld from the Palisades reactor as a function of temperature for the unirradiated and irradiated conditions at neutron fluences of 1.4 and 3.4×10^{23} n m^{-2}.

the Palisades reactor was 27 °C higher than that observed in the weld from the Midland reactor that was irradiated to the same fluence of 3.4×10^{23} n m^{-2} ($E > 1$ MeV).

3.2. Microstructural characterization

Atom probe tomography revealed that there were no fine intragranular precipitates in the unirradiated weld material from the Midland reactor. The matrix copper level was estimated to be 0.11 at.% Cu. This value is consistent with the previous atom probe characterization of this unirradiated weld [24]. This value is lower than the alloy composition due to the formation of coarse copper precipitates on grain boundaries and dislocations during the stress relief treatment.

A high number density, 5×10^{23} m^{-3}, of copper-, nickel-, manganese-, silicon- and phosphorus-enriched precipitates was observed in the Midland weld that was irradiated to a fluence of 3.4×10^{23} m^{-2}, ($E > 1$ MeV), as shown in Fig. 3. Several dislocations are also evident in these atom maps from the linearly distributed solute segregation. A set of high resolution atom maps of an individual precipitate is shown in Fig. 4. These atom maps reveal that the extents of the manganese, nickel and silicon atoms are larger than that of copper atoms. In this precipitate, some phosphorus atoms are concentrated at the core of the precipitate. However, the behavior of phosphorus was found to vary with some precipitates containing few if any phosphorus atoms and some precipitates exhibiting phosphorus segregation to the interface. Although not readily apparent in the atom map shown in Fig. 4 due to their depletions, molybdenum, chromium and carbon were not found to be associated with the precipitates but partitioned to the ferrite matrix. No other ultrafine precipitates were observed in this weld.

From the maximum separation method based on a d_{max} parameter of 0.6 nm for copper atoms and a n_{min} parameter of 10 atoms, the radius of gyration of these precipitates was found to vary between 0.5 and ~1.3 nm for the high fluence Midland weld, as shown in Fig. 5. The average radius of gyration of 222 precipitates was estimated to be 0.87 ± 0.17 nm. This yields an average Guinier radius of 1.1 ± 0.2 nm. Both these estimates are slightly underestimates due to the difference in magnification between the precipitates and the surrounding matrix caused by their different evaporation fields.

The compositions of the core of these precipitates, as estimated from the maximum separation envelope method with a grid size of 0.1 nm, are shown schematically in Fig. 6. In this figure, the compositions have been sorted in terms of their increasing size. The average composition of the core of these precipitates was estimated to be

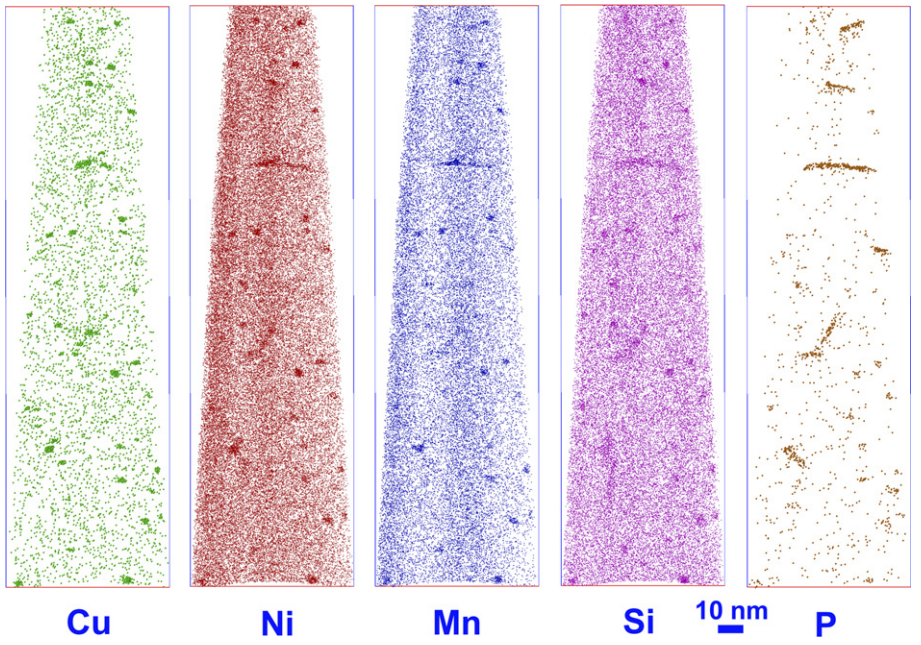

Fig. 3. Atom map of the solute distribution in the high fluence (3.4×10^{23} n m^{-2} ($E > 1$ MeV)) weld from the Midland reactor. Several dislocations with phosphorus segregation and a high number density of copper-, nickel-, manganese-, silicon- and phosphorus-enriched precipitates are evident. The box enclosing the data is $63 \times 60 \times 228$ nm.

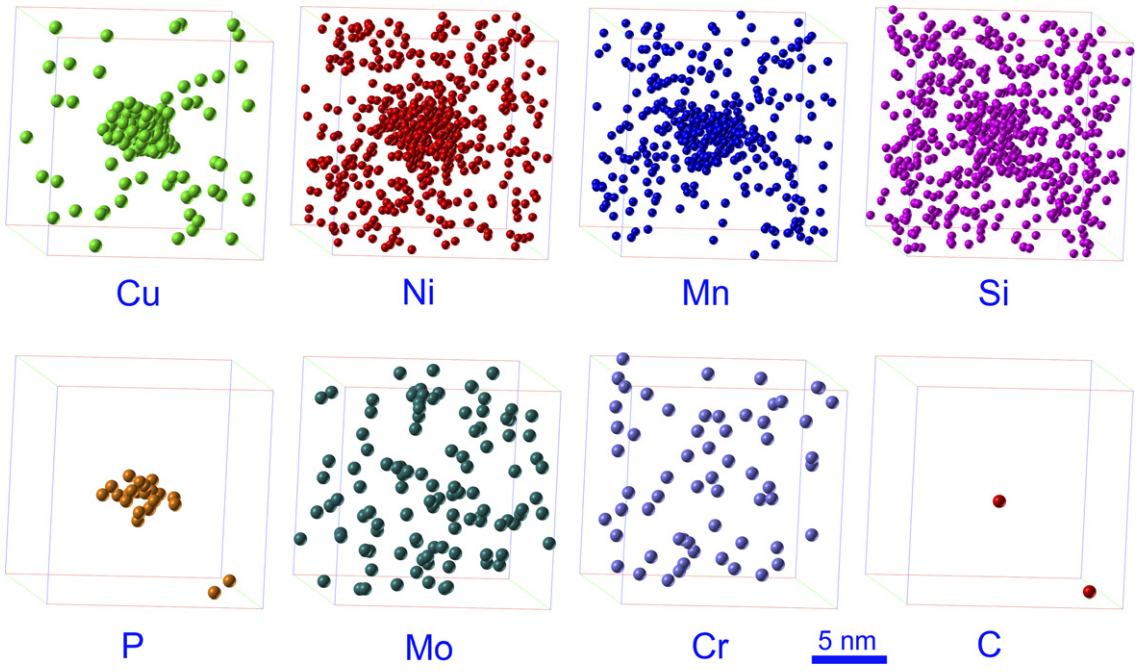

Fig. 4. Atom maps of an individual copper-, nickel-, manganese-, silicon- and phosphorus-enriched precipitate in the high fluence weld (3.4×10^{23} n m^{-2} ($E > 1$ MeV)) from the Midland reactor. Note the extents of the nickel, manganese and silicon atoms are larger than that of the copper atoms.

$83.4 \pm 5.1\%$ Cu, $1.2 \pm 0.9\%$ Ni, $0.8 \pm 0.6\%$ Mn, 0.7 ± 0.6 % Si.

An averaged radial concentration profile from several of these precipitates from the center of mass

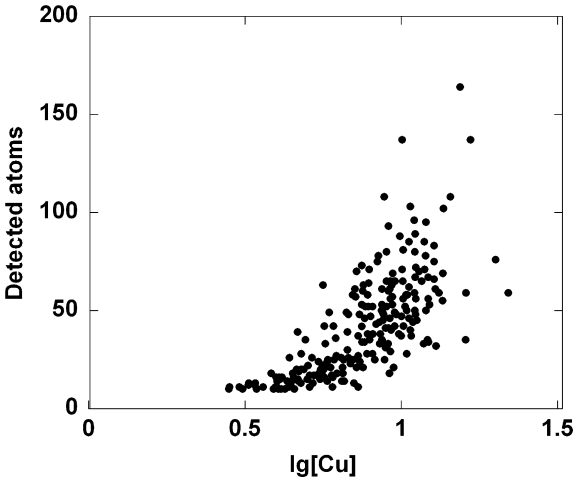

Fig. 5. The distribution in the radii of gyration of the copper-, nickel-, manganese-, silicon- and phosphorus-enriched precipitates in the high fluence (3.4×10^{23} n m^{-2} ($E > 1$ MeV)) weld from the Midland reactor as estimated by the maximum separation method. These data are not corrected for the variation in local magnification between the matrix and the precipitate.

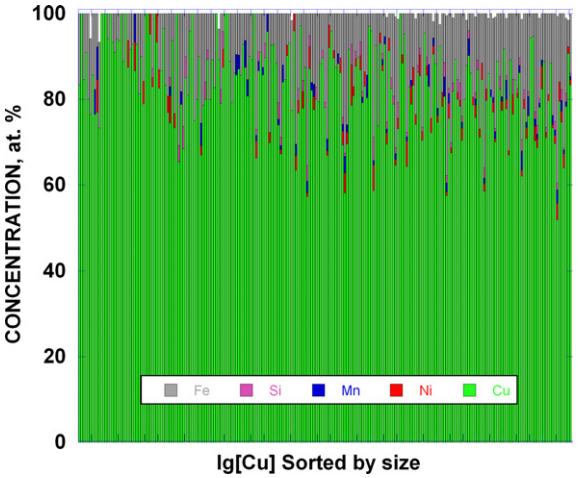

Fig. 6. The compositions of the copper-, nickel-, manganese-, silicon- and phosphorus-enriched precipitates in the high fluence (3.4×10^{23} n m^{-2} ($E > 1$ MeV)) weld from the Midland reactor as estimated by the maximum separation envelope method. The data are sorted by increasing size of the precipitates.

into the matrix for copper, nickel, manganese and silicon is shown in Fig. 7. The partitioning of nickel, manganese and silicon to both the core of the precipitate and the precipitate–matrix interface is evident. A slight tail of these solutes into the matrix is also evident.

These copper-enriched precipitates were observed both in the matrix of the weld and also

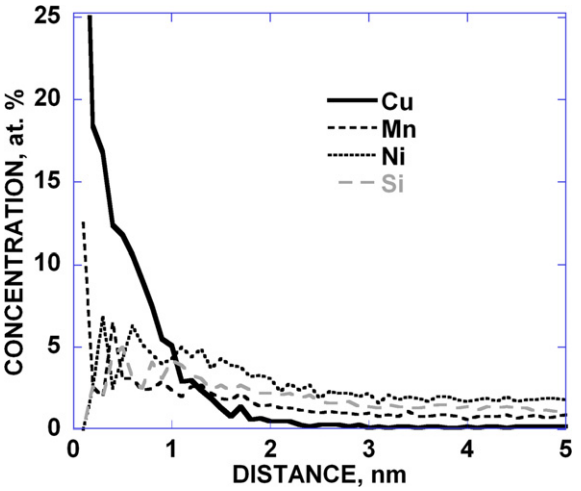

Fig. 7. Average radial concentration profile from the centre of mass of the copper-enriched precipitates out into the ferrite matrix for the weld from the Midland reactor that was irradiated to a fluence of 3.4×10^{23} n m^{-2} ($E > 1$ MeV).

preferentially located along the dislocations, as shown in Figs. 8 and 9. No appreciable difference was observed in the sizes or the compositions of the precipitates in the matrix and on the dislocations. The average interparticle distance along the dislocations was estimated to be 11 ± 3 nm. Phosphorus segregation was also evident along the dislocations, as shown in Figs. 8 and 9. A two-dimensional phosphorus concentration map of the region near the dislocation shown in Fig. 9, is shown

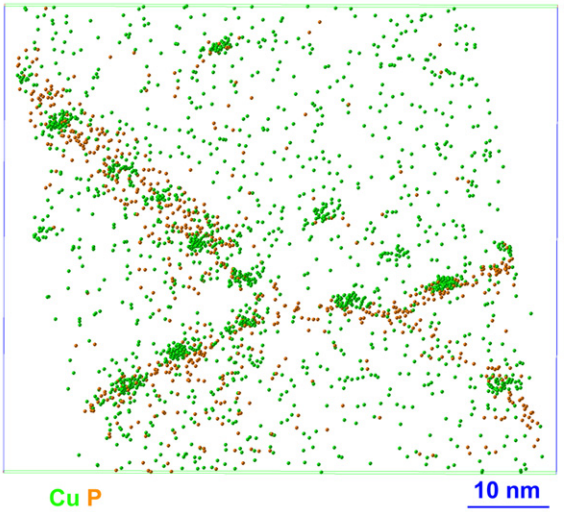

Fig. 8. Atom map of a dislocation network in the high fluence (3.4×10^{23} n m^{-2} ($E > 1$ MeV)) weld from the Midland reactor that exhibits phosphorus segregation and a high number of copper- and phosphorus-enriched precipitates.

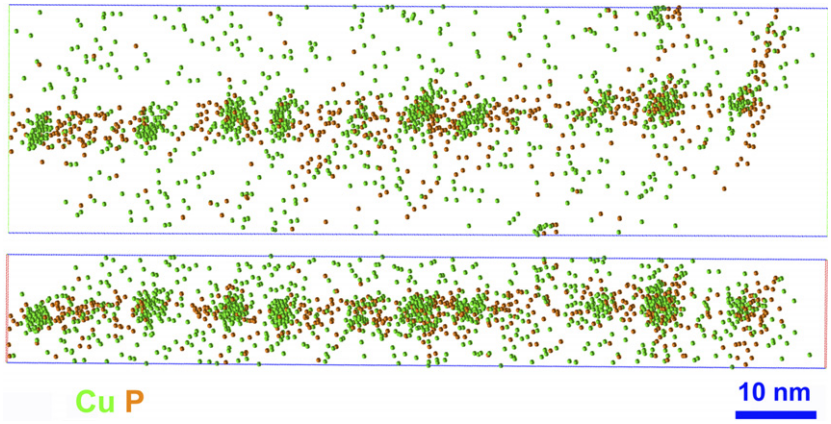

Fig. 9. Atom maps (plan and size views) of a dislocation in the high fluence (3.4×10^{23} n m^{-2} ($E > 1$ MeV)) weld from the Midland reactor that exhibits phosphorus segregation and a high number of copper- and phosphorus-enriched precipitates.

in Fig. 10. The phosphorus enrichment was typically ~1 at.% P with local maxima of up to ~2.5 at.% P. This represents phosphorus enrichments of ~30–80 times the alloy phosphorus content.

As in the unirradiated weld from the Midland reactor, no fine intragranular precipitates were observed in the unirradiated weld material from the Palisades reactor. However, high number

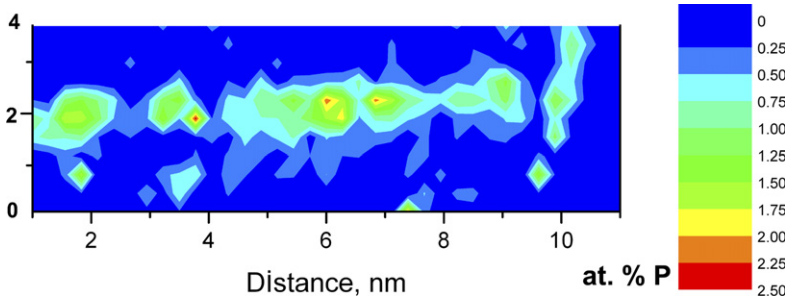

Fig. 10. Tracer map of the phosphorus concentration of the dislocation shown in Fig. 9 in the high fluence (3.4×10^{23} n m^{-2} ($E > 1$ MeV)) weld from the Midland reactor.

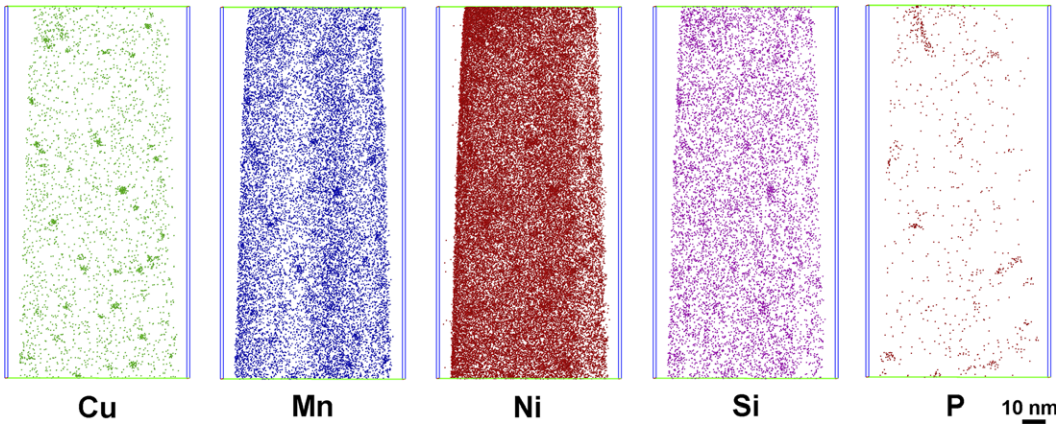

Fig. 11. Ten nanometer-thick atom map slices of the solute distribution in the low fluence (1.4×10^{23} n m^{-2} ($E > 1$ MeV)) weld from the Palisades reactor. A high number density of ultrafine copper-, nickel-, manganese-, silicon- and phosphorus-enriched precipitates are evident. A phosphorus-enriched dislocation is also evident.

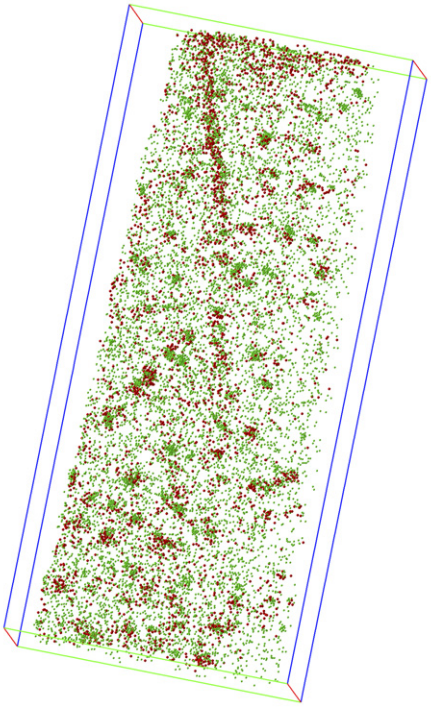

Fig. 12. Atom map of the solute distribution in the low fluence (1.4×10^{23} n m^{-2} ($E > 1$ MeV)) weld from the Palisades reactor. Copper atoms are green and phosphorus atoms are brown. A high number density of ultrafine copper-, nickel-, manganese-, silicon- and phosphorus-enriched precipitates and a dislocation exhibiting phosphorus segregation are evident. The box enclosing the data is $64 \times 63 \times 140$ nm. (For interpretation of the references in color in this figure legend, the reader is refered to the web version of this article.)

densities, $\sim 5 \times 10^{23}$ m^{-3}, of copper-, nickel-, manganese-, silicon- and phosphorus-enriched precipitates were observed in the low fluence (1.4×10^{23} m^{-2}, $E > 1$ MeV) weld material, from the Palisades reactor as shown in Figs. 11 and 12. Similarly, high number densities, $\sim 7 \times 10^{23}$ m^{-3}, of copper-, nickel-, manganese-, silicon- and phosphorus-enriched precipitates were observed in the high fluence (3.4×10^{23} m^{-2}, $E > 1$ MeV) weld material, as shown in Figs. 13 and 14. As in the Midland reactor, the extents of the nickel, manganese and silicon atoms were larger than that of the copper atoms, as shown in the high resolution atom maps from the high fluence weld from the Palisades reactor in Fig. 14. No other ultrafine precipitates were observed in this neutron irradiated weld.

From the maximum separation method based on a d_{max} parameter of 0.6 nm for copper atoms and a n_{min} parameter of 10 atoms, the radius of gyration of these precipitates was found to vary between 0.5 and $\sim$1.3 nm for the high fluence (3.4×10^{23} m^{-2}, $E > 1$ MeV) weld from the Palisades reactor, as shown in Fig. 15. This range was similar to the precipitates in the similar fluence weld from the Midland reactor. The average radius of gyration of 196 precipitates was estimated to be 0.81 ± 0.16 nm. This yields an average Guinier radius of 1.0 ± 0.2 nm. In the low fluence (1.4×10^{23} m^{-2}, $E > 1$ MeV) weld from the Palisades reactor, the average radius of gyration and Guinier radius of

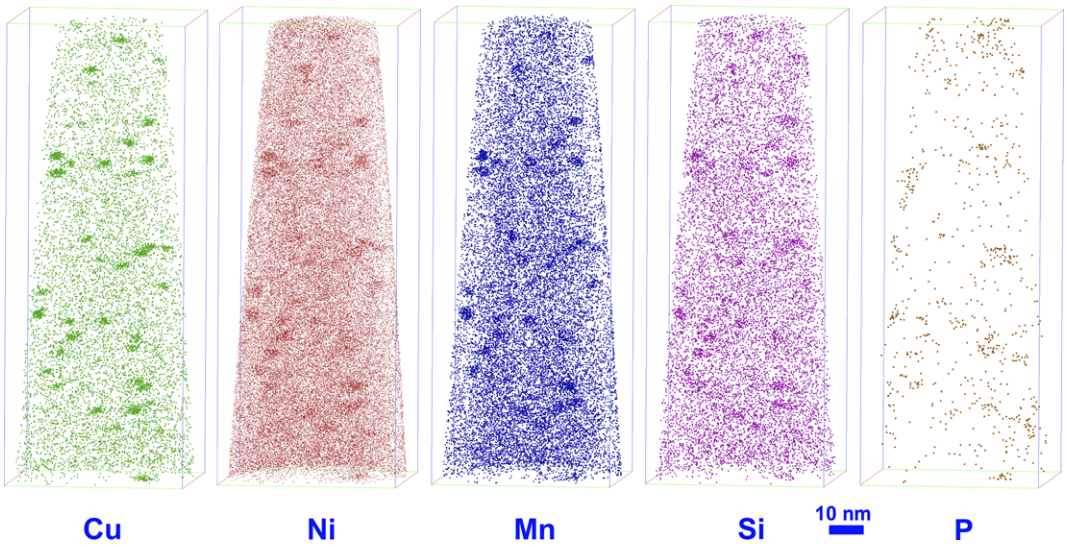

Fig. 13. Atom maps of the solute distribution in the high fluence (3.4×10^{23} n m^{-2} ($E > 1$ MeV)) weld from the Palisades reactor. A high number density of copper-, nickel-, manganese-, silicon- and phosphorus-enriched precipitates are evident. The box enclosing the data is $42 \times 41 \times 105$ nm.

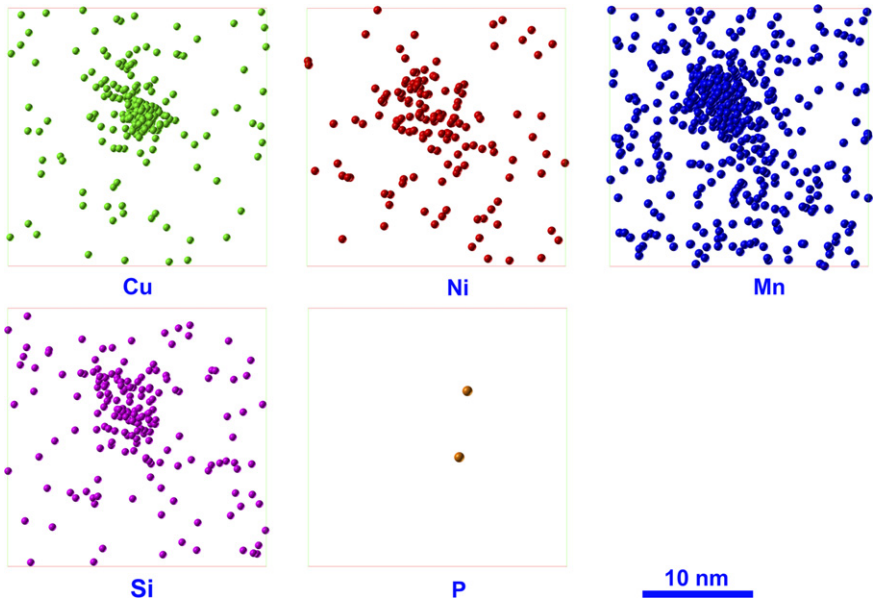

Fig. 14. Atom maps of an individual copper-, nickel-, manganese-, silicon- and phosphorus-enriched precipitate in the high fluence weld (3.4×10^{23} n m^{-2} ($E > 1$ MeV)) from the Palisades reactor. Note the extents of the nickel, manganese and silicon atoms are larger than that of the copper atoms.

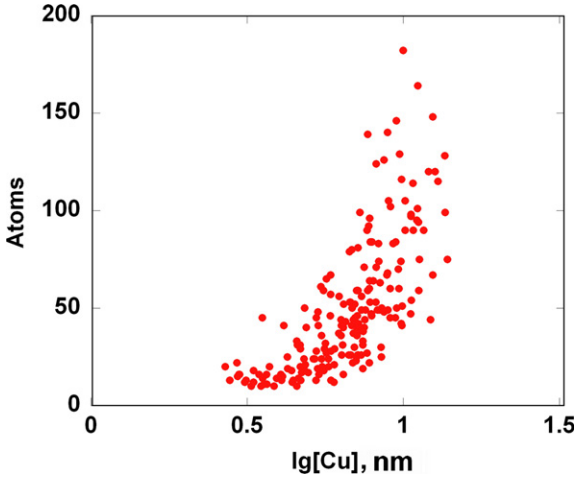

Fig. 15. The distribution in the radii of gyration of the copper-, nickel-, manganese-, silicon- and phosphorus-enriched precipitates in the high fluence (3.4×10^{23} n m^{-2} ($E > 1$ MeV)) weld from the Palisades reactor as estimated by the maximum separation method. These data are not corrected for the variation in local magnification between the matrix and the precipitate.

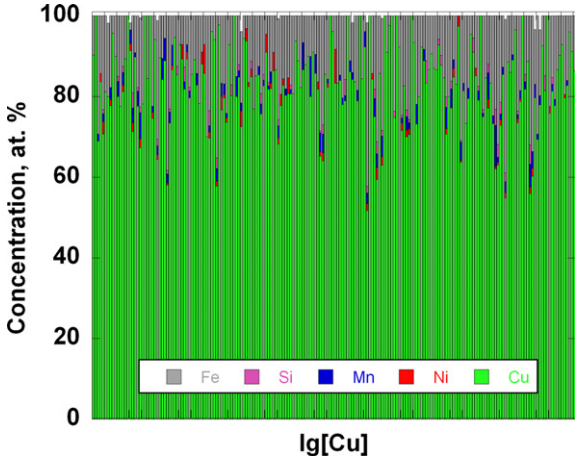

Fig. 16. The compositions of the copper-, nickel-, manganese-, silicon- and phosphorus-enriched precipitates in the high fluence (3.4×10^{23} n m^{-2} ($E > 1$ MeV)) weld from the Palisades reactor as estimated by the maximum separation envelope method. The data are sorted by increasing size of the precipitates.

precipitates was estimated to be 0.72 ± 0.13 nm and 1.0 ± 0.2 nm, respectively. These estimates are slightly underestimated due to the difference in magnification between the precipitates and the surrounding matrix due to their different evaporation fields.

The compositions of the core of these precipitates, as estimated from the maximum separation envelope method with a grid size of 0.1 nm, are shown schematically in Fig. 16. In this figure, the compositions have been sorted in terms of their increasing size. The average composition of the core of these precipitates was estimated to be Fe – 83 ± 10 at.% Cu, 2.3% Ni, 1.5% Mn, 0.5% Si.

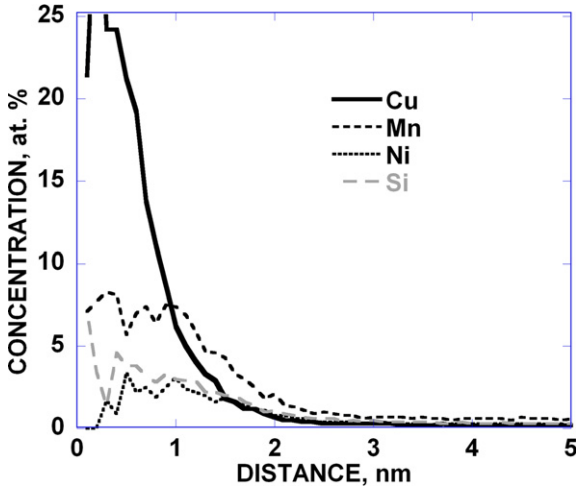

Fig. 17. Average radial concentration profile from the centre of mass of the copper-enriched precipitates out into the ferrite matrix for the weld from the Palisades reactor that was irradiated to a fluence of 3.4×10^{23} n m^{-2} ($E > 1$ MeV).

An averaged radial concentration profile from several of these precipitates from the center of mass into the matrix for copper, nickel, manganese and silicon is shown in Fig. 17. The partitioning of nickel, manganese and silicon to both the core of the precipitate and the precipitate–matrix interface is evident. A slight tail of these solutes into the matrix is also evident.

A series of 20-nm-thick atom maps of a selected volume containing a dislocation in the high fluence (3.4×10^{23} n m^{-2} ($E > 1$ MeV)) weld from the Palisades reactor is shown in Fig. 18. Carbon and phosphorus segregation to different segments of the dislocation are clearly evident. A high number of copper-, nickel-, manganese-, silicon- and phosphorus-enriched precipitates are also observed along the line of the dislocation. The average interparticle distance along the dislocation, ~10 nm, was similar to that in the midland weld. A two-dimensional phosphorus concentration map of this region near the dislocation is shown in Fig. 19. The phosphorus enrichment was typically about 1 at.% P with local maxima of up to ~2.5 at.% P. This represents phosphorus enrichments of ~30–80 times the alloy phosphorus content. This phosphorus enrichment was similar to that found in the weld from the Midland reactor.

4. Discussion

A comparison of the fracture toughnesses of the welds from the Midland reactor and Palisades reactor both irradiated to the same fluence of 3.4×10^{23} n m^{-2} ($E > 1$ MeV) indicates that the experimentally observed ΔT_{41J} Charpy shift was 41 °C higher and the experimentally observed fracture toughness T_0 shift was 27 °C higher in the higher nickel weld from the Palisades reactor. Assuming that all other factors were equivalent in these two welds, then the additional nickel produces a significant change in the mechanical properties of the weld. However, the other differences in alloy composition, in particular the different manganese and silicon levels, makes a complete interpretation far more complex.

Atom probe tomography revealed that the intragranular microstructures of the welds from the Midland reactor and Palisades reactor both irradiated to the same fluence of 3.4×10^{23} n m^{-2} ($E > 1$ MeV) were generally similar. Both materials contained high number densities of ultrafine copper-, manganese-, silicon- and phosphorus-enriched precipitates, with preferential precipitation along and similar levels of phosphorus segregation to the dislocations. No other intragranular precipitates were observed in either material. The average radius of gyration and Guinier radius of the ultrafine copper-, manganese-, silicon- and phosphorus-enriched precipitates in the weld from the Midland reactor were 0.87 ± 0.17 nm and 1.1 ± 0.2 nm, respectively compared to 0.81 ± 0.16 nm and 1.0 ± 0.2 nm, respectively, in the weld from the Palisades reactor. Although a slight decrease is apparent in the average size, the large standard deviation due to precipitate-to-precipitate variations indicates that they are not statistically different. Unfortunately, even small differences in size at this nanometer size range could have a significant influence on the effectiveness of pinning dislocations as there are comparatively large differences in the absolute number of atoms in the precipitates. Small differences were detected in the number densities of the ultrafine copper-, manganese-, silicon- and phosphorus-enriched precipitates. The larger ΔT_{41J} shift of 149° in the higher nickel weld from the Palisades reactor versus the ΔT_{41J} shift of 117 °C in the weld from the Midland reactor for the same neutron fluence of 3.4×10^{23} m^{-2} ($E > 1$ MeV) was correlated with a slightly higher number density of slightly smaller copper-enriched precipitates.

As the segments of the dislocations between the precipitates were straight and not scalloped and because the distribution of the precipitates was linearly aligned, it is likely that the copper-enriched

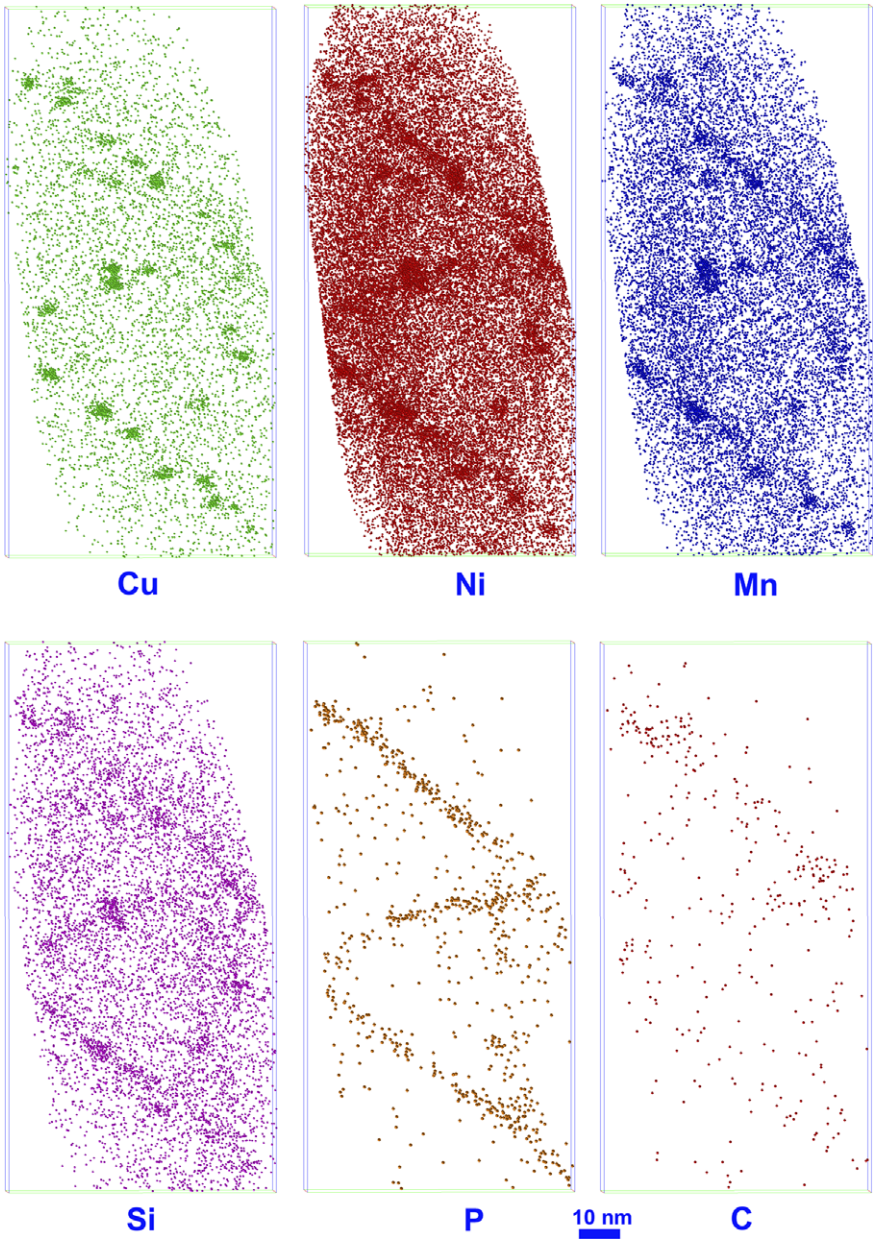

Fig. 18. Atom maps of a dislocation in the high fluence (3.4×10^{23} n m^{-2} ($E > 1$ MeV)) weld from the Palisades reactor that exhibits phosphorus segregation and a high number of copper-, nickel-, manganese-, silicon- and phosphorus-enriched precipitates. Carbon and phosphorus segregation to the dislocation are evident.

precipitates were nucleated heterogeneously on pre-existing dislocations rather than the precipitates acting as pinning sites for glissile dislocations. The higher number density of precipitates along the dislocations compared to the matrix also indicates that the precipitates were nucleated on pre-existing dislocations. The similar size of the precipitates in the matrix and on the dislocation would suggest that they nucleated at the same time as the intragranular precipitates and early in the exposure to radiation. Enhanced growth due to piped diffusion along the dislocation probably was not a significant factor due to close proximity of the precipitates along the dislocations.

The preferential precipitation of the copper-enriched precipitates on and the phosphorus and

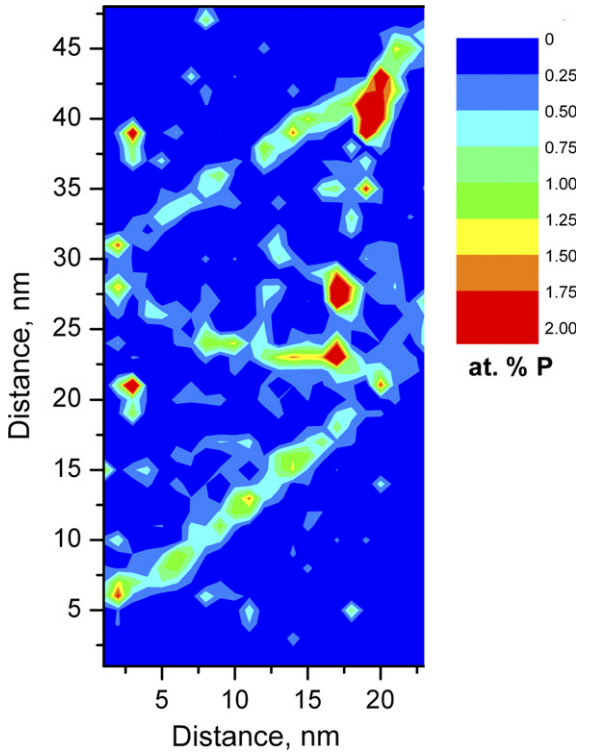

Fig. 19. Two-dimensional concentration map of the phosphorus distribution for the dislocation in the high fluence (3.4×10^{23} n m^{-2} ($E > 1$ MeV)) weld from the Palisades reactor.

carbon segregation to the dislocation will effectively pin these dislocations from movement. In order for these dislocations to move, they will have to bow around or cut through the precipitates and unpin themselves from the solute segregation. These processes will be energetically unfavorable. Additionally, these pinned dislocations will act as barriers for glissile dislocations thereby influencing the mechanical properties. However, the relative importance of the pinned dislocations with their associated copper-enriched precipitates versus the matrix copper-enriched precipitates as barriers to the movement of new glissile dislocations remains to be established. Therefore, the preexisting dislocation densities may be an additional factor in mechanical properties after neutron irradiation.

Other changes in the microstructure such as solute segregation to the lath and grain boundaries that could also significantly impact the mechanical properties were not investigated in this study. It is possible that the increase in nickel could also have a synergistic increase in the phosphorus level at the grain and lath boundaries leading to enhanced embrittlement as found in temper embrittlement.

5. Summary

This atom probe tomography characterization of the welds from the high nickel and copper Midland and Palisades reactors after neutron irradiation to fluences up to 3.4×10^{23} m^{-2} ($E > 1$ MeV) has revealed high number densities of ~2-nm-diameter copper-, nickel-, manganese- and silicon-enriched precipitates. These copper-enriched precipitates were found in both the matrix and also preferentially on the dislocations. The dislocations were also decorated with phosphorus and carbon. No other nanoscale precipitates were observed in these welds. For the same neutron fluence of 3.4×10^{23} m^{-2} ($E > 1$ MeV), the higher nickel weld from the Palisades reactor had a higher ΔT_{41J} shift of 149 °C compare to a shift of 117 °C in the weld from the Midland reactor. This larger shift in the ductile–brittle transformation temperature was correlated with a slightly higher number density of slightly smaller copper-enriched precipitates.

Acknowledgements

Research at the Oak Ridge National Laboratory SHaRE User Center was sponsored by the Division of Materials Sciences and Engineering, US Department of Energy, under contract DE-AC05-00OR22725 with UT-Battelle, LLC and by the Office of Nuclear Regulatory Research, US Nuclear Regulatory Commission under inter-agency agreement DOE 1886-N695-3W with the US Department of Energy. The authors acknowledge the Charpy impact and fracture testing by E. Manneschmidt and R. Swain.

References

[1] A.M. Kryukov, Y.A. Nikolaev, A.V. Nikolaeva, Nucl. Eng. Des. 186 (1998) 353.
[2] T.J. Williams, P.R. Burtz, C.A. English, P.H.N. de la Cour Ray, in: G.J. Theus, J.R. Weeks (Eds.), 3rd International Symposium on Environmental Degradation of Materials in Nuclear Power Systems—Water Reactors, 1987, 1988, p. 121.
[3] G.R. Odette, G.E. Lucas, in: L.E. Steele (Ed.), Irradiation Embrittlement of Reactor Pressure Vessel Steels: An International Review: ASTM STP 909, ASTM, 1986, p. 206.
[4] G.R. Odette, G.E. Lucas, in: N.H. Packan, R.E. Stoller, A.S. Kumar (Eds.), Effects of Radiation on Materials: 14th International Symposium, ASTM STP 1046, vol. II, American Society for Testing and Materials, Philadelphia, 1990, p. 323.

[5] G.R. Odette, in: Microstructure of Irradiated Materials, MRS Symposium Proceedings, vol. 373, Pittsburgh, PA, 1995, p. 137.
[6] R. Gerard et al., in: David S. Gelles, Randy K. Nanstad, Arvind S. Kumar, Edward A. Little (Eds.), Effects of Radiation on Materials: 17th International Symposium, ASTM STP 1046, vol. II, American Society for Testing and Materials, 1996, p. 294.
[7] G.R. Odette, C.L. Liu, B.D. Wirth, in: Microstructure Evolution during Irradiation, MRS Soc. Symposium Proceedings, vol. 439, Pittsburgh, 1997, p. 457.
[8] Y.A. Nikolaev et al., J. Nucl. Mater. 226 (1995) 144.
[9] M.K. Miller, Atom Probe Tomography, Kluwer Academic/Plenum, New York, NY, 2000.
[10] M.K. Miller, A. Cerezo, M.G. Hetherington, G.D.W. Smith, Atom Probe Field Ion Microscopy, Oxford University, Oxford, UK, 1996.
[11] M.K. Miller, P. Pareige, M.G. Burke, Mater. Charact. 44 (2000) 235.
[12] M.K. Miller, M.G. Hetherington, M.G. Burke, Metall. Trans. 20A (1989) 2651.
[13] M.K. Miller, P. Pareige, in: G.E. Lucas, L. Snead, M.A. Kirk Jr., R.G. Elliman (Eds.), Proceedings of the MRS 2000 Fall Meeting, Symposium R: Microstructural Processes in Irradiated Materials, Boston, MA, 27–30 November 2000, vol. 650, Materials Research Society, Pittsburgh, PA, 2001, p. R6.1.1.
[14] J.M. Hyde, C.A. English, in: G.E. Lucas, L. Snead, M.A. Kirk Jr., R.G. Elliman (Eds.), Proceedings of the MRS 2000 Fall Meeting, Symposium R: Microstructural Processes in Irradiated Materials, Boston, MA, 27–30 November 2000, vol. 650, Materials Research Society, Pittsburgh, PA, 2001, p. R6.6.1.
[15] M.K. Miller, K.F. Russell, P. Pareige, in: G.E. Lucas, L. Snead, M.A. Kirk Jr., R.G. Elliman (Eds.), Proceedings of the MRS 2000 Fall Meeting, Symposium R: Microstructural Processes in Irradiated Materials, Boston, MA, 27–30 November 2000, vol. 650, Materials Research Society, Pittsburgh, PA, 2001, p. R3.15.1.
[16] M.K. Miller, K.F. Russell, J. Kocik, E. Keilova, J. Nucl. Mater. 282 (2000) 83.
[17] M.K. Miller, K.F. Russell, J. Kocik, E. Keilova, Micron 32 (2001) 749.
[18] M.K. Miller, S.S. Babu, M.A. Sokolov, R.K. Nanstad, S.K. Iskander, Mater. Sci. Eng. A 327 (2002) 76.
[19] M.K. Miller, M.A. Sokolov, R.K. Nanstad, S.K. Iskander, in: Proc. 10th Int. Conf. on Environmental Degradation of Materials in Nuclear Power Systems – Water Reactors, Lake Tahoe, NV, 5–9 August 2001, pub. NACE, 2002.
[20] M.G. Burke, R.J. Stofanak, J.M. Hyde, C.A. English, W.L. Server, in: Proc. 10th Int. Conf. on Environmental Degradation of Materials in Nuclear Power Systems – Water Reactors, Lake Tahoe, NV, 5–9 August 2001, pub. NACE, 2002.
[21] R.G. Carter, N. Soneda, K. Dohi, J.M. Hyde, C.A. English, W. Server, J. Nucl. Mater. 298 (2001) 211.
[22] P. Auger, P. Pareige, S. Welzel, J.C. Van Duysen, J. Nucl. Mater. 280 (2000) 331.
[23] J.M. Hyde, D. Ellis, C.A. English, T.J. Williams, in: S.T. Rosinski, M.L. Grossbeck, T.R. Allen, A.S. Kumar (Eds.), 20th Int. Conf. Effects of Radiation on Materials, ASTM STP 1405, American Society for Testing and Materials, West Conshohocken, PA, 2001, p. 262.
[24] M.K. Miller, M.A. Sokolov, R.K. Nanstad, K.F. Russell, J. Nucl. Mater. 351 (2006) 187.
[25] M.K. Miller, K.F. Russell, J. Nucl. Mater. 250 (1997) 223.
[26] M.K. Miller, in: A. Gonis, P.E.A. Turchi, A.J. Ardell (Eds.), Proceedings of the MRS 1999 Fall Meeting, Symposium E: Nucleation and Growth Process in Materials, Boston, MA, November 29–December 2, 1999, vol. 580, Materials Research Society, Warrendale, PA, 2000, p. 35.
[27] M.K. Miller, B.D. Wirth, G.R. Odette, Mater. Sci. Eng. A. A353 (2003) 133.